Magnetism of ordered and disordered Ni_2MnAl full Heusler compounds

E. Simon,[1] J. Gy. Vida,[1] S. Khmelevskyi,[1] and L. Szunyogh[1,2]
[1]*Department of Theoretical Physics, Budapest University of Technology and Economics, Budafoki út 8., H-1111 Budapest, Hungary*
[2]*MTA-BME Condensed Matter Research Group, Budafoki út 8, H-1111 Budapest, Hungary*
(Received 18 June 2015; published 28 August 2015)

Based on *ab initio* calculations and Monte Carlo simulations, we present a systematic study of the magnetic ground state and finite temperature magnetism of ordered and disordered Ni_2MnAl full Heusler compounds. By increasing the degree of the long-range chemical disorder between the Mn and Al sublattices, the magnetic order progressively changes from the ferromagnetic state in the ordered $L2_1$ phase toward a fully compensated antiferromagnetic state in the disordered $B2$ phase and we also conclude that the Ni atoms exhibit induced moments. We determine the Mn-Mn interactions by using the magnetic force theorem and find dominating, but rather weak ferromagnetic couplings in the ordered $L2_1$ phase. We used a recently proposed renormalization technique to include the weak Ni moments into the spin model, which indeed remarkably increased the nearest-neighbor Mn-Mn interaction. In accordance with the total energy calculations, in the disordered compounds, strong antiferromagnetic site-antisite Mn-Mn interactions appear. Determining the spin-spin correlation functions from Monte Carlo simulations, we conclude that above the transition temperature, short-range antiferromagnetic correlations prevail between the Mn atoms. In view of the potential application of disordered Ni_2MnAl as a room temperature antiferromagnet, we calculate the magnetic anisotropy energies of tetragonally distorted samples in the $B2$ phase and find that they are smaller by two orders in magnitude than in the frustrated antiferromagnet $IrMn_3$.

DOI: 10.1103/PhysRevB.92.054438 PACS number(s): 71.20.Be, 75.20.En, 71.70.Gm

I. INTRODUCTION

The growing interest in new metallic antiferromagnets, triggered by their application in spintronic devices [1,2], focused attention to antiferromagnetic (AFM) Heusler alloys [3,4]. However, relatively few AFM Heusler alloys are known with sufficiently high Néel temperatures (T_N) [5]. For instance, the Néel temperatures of the AFM Ru_2MnSi and Ru_2MnGe compounds are slightly above room temperature (313 and 316 K, respectively) [6]. Recently, the antiferromagnetism in Ru_2MnZ alloys (Z = Sb, Sn, Si, Ge) has been discussed, together with the possibility to increase T_N of Ru_2MnSi [7]. Since the Néel temperature of the Ni_2MnAl compound in the disordered $B2$ phase is also higher than the room temperature (313 K) [8], the investigation of the antiferromagnetism in Ni_2MnAl raises interest due to its prospective application as a pinning material in exchange bias devices.

The Ni_2MnAl compound has been a subject of broad experimental [8–13] and theoretical investigations [14–17]. It is known from experiments that Ni_2MnAl has a strong tendency to chemical disorder in the Mn-Al sublattices [8,10]. In the well ordered samples close to the $L2_1$ (full Heusler) phase the magnetic ordering is ferromagnetic. This was confirmed by first-principles calculations [14], and it has also been shown that the ferromagnetic order is stable in the $Ni_2Mn_xAl_{1-x}$ alloys for concentrations between $x = 0.14$ to 0.31 [15]. In the $B2$ phase, the Mn and Al atoms occupy randomly the sites of the Mn and Al sublattices of the $L2_1$ structure. A continuous transition between the $L2_1$ and $B2$ structures can be achieved by introducing compositions $Mn_{1-x}Al_x$ and $Al_{1-x}Mn_x$ ($0 \leqslant x \leqslant 0.5$) on the pristine Mn and Al sublattices, respectively. Quite clearly, $x = 0$ corresponds to the ordered $L2_1$ structure, while $x = 0.5$ to the disordered $B2$ structure. Note that the Mn atoms at the sites of the original Mn or Al sublattices are referred to occupy, in order, site (S) or antisite (AS) positions. The site and antisite positions of Mn atoms are sketched in Fig. 1. It can be seen that in this structure the distance for the nearest-neighbor (NN) site-antisite atoms is $a/2$, while the NN distance between the pairs of site or antisite atoms is $a/\sqrt{2}$, where a denotes the lattice constant.

Despite of intensive experimental research, the magnetic state of Ni_2MnAl is still controversial. The experimental investigations show that the magnetic state strongly depends on the heat treatment and it is difficult to achieve the perfectly ordered $L2_1$ structure [8,10–12]. A mixed $B2/L2_1$ geometry of the Ni_2MnAl also exists and it was used in the granular films to produce negative magnetic resistance [13].

Two artificially ordered $B2$ phases have been examined by first-principles calculations [16]. In the so-called $B2$-I and $B2$-II structures, the Mn and Al atoms are ordered into alternating layers along the (001) and (110) directions, respectively. In both cases, antiferromagnetic ordering of the Mn moments was found. However, so far, no attempt was done in the literature to provide a detailed *ab initio* investigation of the magnetic ordering in the disordered $B2$ phase, as well as for the partially disordered compounds between the ordered $L2_1$ and fully disordered $B2$ phases.

In this work, using *ab initio* calculations we study the disordered $Ni_2(Mn_{1-x}Al_x)(Al_{1-x}Mn_x)$ ($0 \leqslant x \leqslant 0.5$) full Heusler compounds. First, we perform self-consistent calculations to obtain the energetically favorable magnetic state and the spin-magnetic moments. In agreement with previous theoretical work [15], we find that the ground state is the ferromagnetic $L2_1$ phase and by increasing the amount of Mn atoms in the antisite position, the AFM state becomes lower in energy than the FM state. The moment of the Ni atoms appears to be proportional with the average moment of the Mn atoms indicating that in this system the Ni atoms have weak moments. We then calculated the exchange parameters between the Mn atoms using the magnetic force theorem [18] and performed

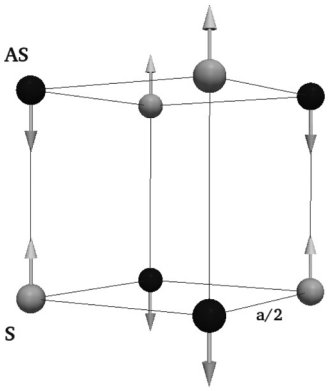

FIG. 1. Site (S) and antisite (AS) positions of the Mn atoms occupying positions of the originally pure Mn and Al sublattices with compositions of $Mn_{1-x}Al_x$ and $Al_{1-x}Mn_x$, respectively. The arrows indicate the orientation of the corresponding spin-moments in the AFM state.

Monte Carlo simulations to explore the finite temperature equilibrium properties. From the Monte Carlo simulation, we find that for the atomically ordered $L2_1$ phase, the Curie temperature is smaller than the experimental one, most likely as a consequence of neglected longitudinal fluctuations of the Ni moments. In order to take this effect into account, we apply a recently proposed renormalization technique [19] for the Mn-Mn exchange parameters in the FM $L2_1$ phase. In case of atomic disorder, the site-antisite Mn-Mn interactions appear to have AFM character, favoring an AFM state in agreement with the total energy calculations. We also evaluate spin-spin correlation functions and find that a finite correlation persists above the transition temperature for the nearest and next nearest Mn site-antisite neighbors. Finally, we calculate the magnetic anisotropy energy for the disordered $B2$ phase, as well as for the ordered $B2$-I and $B2$-II pseudophases.

II. COMPUTATIONAL METHOD

In terms of the fully relativistic screened Korringa-Kohn-Rostoker (SKKR) Green's function method [20,21], we performed self-consistent calculations of bulk $Ni_2(Mn_{1-x}Al_x)$ $(Al_{1-x}Mn_x)$ Heusler alloys with x ranging from 0 to 0.5. For the disordered cases, we employed the single-site coherent potential approximation (CPA). Overall, we used the experimental lattice constant, $a = 5.812$ Å, the local spin-density approximation (LSDA) as parametrized by Vosko *et al.* [22] together with the atomic sphere approximation and an angular momentum cutoff of $\ell_{\max} = 2$. The energy integrals were performed by sampling 16 points on a semicircle contour in the upper complex semiplane. We considered ferromagnetic and antiferromagnetic arrangements, where the Mn atoms at the site and antisite positions are aligned antiparallel. By using the self-consistent potentials, we derived the magnetic anisotropy energy (MAE) by means of the magnetic force theorem as a difference of band energies [23–26],

$$E_{\text{anis}} = E_x^{\text{band}} - E_z^{\text{band}}, \tag{1}$$

where the labels x and z refer to the directions of the magnetization (effective field) in the system.

We suppose that the energy of itinerant spin-polarized electron systems can be mapped to a Heisenberg Hamiltonian of classical spins,

$$\mathcal{H} = -\frac{1}{2}\sum_{i,j(i\neq j)} J_{ij}\vec{e}_i\vec{e}_j, \tag{2}$$

where the summation runs over the sites of the lattice, J_{ij} is the exchange interaction, and $\vec{e}_i$ denotes a unit vector along the direction of the magnetic moment at lattice site i. Note that according to Eq. (2) the negative exchange constant means antiferromagnetic coupling, while the positive J_{ij} corresponds to ferromagnetic interaction. It also should be mentioned that due to the $1/2$ factor in the spin Hamiltonian of Eq. (2), our spin-model parameters are twice as large as in previous work [16].

We used two methods to evaluate the parameters of the spin Hamiltonian (2). One of them is the relativistic torque method (RTM) [27,28], which is a relativistic extension of the method of infinitesimal rotations [18], and maps the energy around a specific ordered magnetic configuration. The other one is the spin-cluster expansion (SCE) technique developed by Drautz and Fähnle [29,30], which provides systematic parametrization of the adiabatic energy of an itinerant magnetic system. This method can be combined with the relativistic disordered local moment (DLM) scheme [31–33] to give the exchange interactions in the paramagnetic state [34,35]. Note that both methods are suitable to calculate tensorial exchange parameters [27] but in this work, we use the isotropic component only. Based on the spin model containing the calculated exchange interactions, we performed Monte Carlo (MC) simulations on a lattice of $16 \times 16 \times 16$ unit cells. In general, we used 4×10^5 MC steps to reach the low-temperature equilibrium.

III. RESULTS AND DISCUSSION

A. Total energies and spin magnetic moments

First, we performed self-consistent calculations of the FM and AFM states of $Ni_2(Mn_{1-x}Al_x)$ $(Al_{1-x}Mn_x)$ for several concentrations, $0 \leqslant x \leqslant 0.5$. For the FM state, where the spin-moments of the site and antisite Mn atoms were set parallel to each other, we found that the spin moments of the Ni and Al atoms are oriented parallel and antiparallel to the Mn moments, respectively. In case of the AFM calculations, we fixed the spin-moments of the site and antisite Mn atoms in opposite direction, whereas the spin-moments of the Ni and Al atoms kept their directions as in the FM state. The corresponding total energies are plotted in Fig. 2 as a function of x.

Clearly, the ground state of the Ni_2MnAl compound appears to be the completely ordered $L2_1$ phase. Following previous theoretical findings[14,15], we supposed a FM ground state in this phase. Chemical disorder ($x > 0$) increases the total energy in both the FM and the AFM states. For any degree of disorder, the AFM state is lower in energy than the FM state, indicating that the coupling between the site and antisite Mn atoms is antiferromagnetic. Although the energy of the AFM state of the $B2$ phase decreases by about 37 meV/unit cell as compared to the FM state, this decrease is not sufficient to compensate the energy difference with respect to the ordered

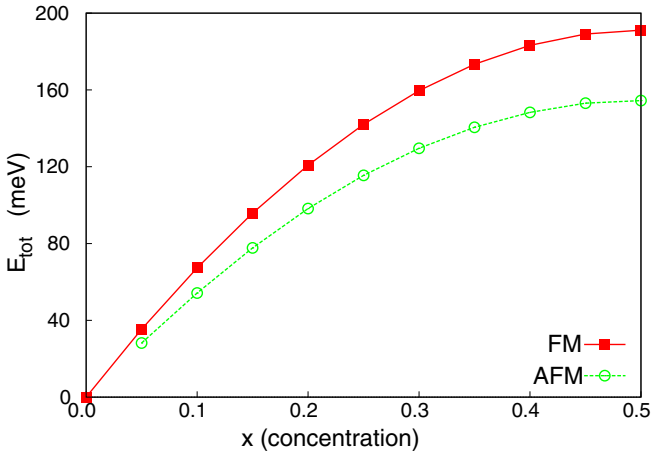

FIG. 2. (Color online) Calculated total energies per formula unit $E_{\rm tot}$ of $Ni_2(Mn_{1-x}Al_x)$ $(Al_{1-x}Mn_x)$ as a function of x in the FM and AFM states. The total energies are normalized to that of the FM $L2_1$ state ($x = 0$).

$L2_1$ phase (∼190 meV/unit cell). Nevertheless, the $B2$ phase can be stabilized at elevated temperatures mainly due to the entropy of mixing and, probably, also to spin-disorder and electronic entropy [36].

The spin moments obtained in the respective magnetic ground states are listed in Table I for different values of x. As can be seen, the moment of the site Mn atoms is just slightly affected by the disorder: the value of $3.32\,\mu_B$ at $x = 0$ increases only to $3.35\,\mu_B$ for $x = 0.5$. The size of the spin moment of the antisite Mn atoms is somewhat more sensitive to the disorder: for small disorder ($x = 0.1$) it has an increased value of $3.46\,\mu_B$ and it gradually decreases to $3.35\,\mu_B$ for the $B2$ phase. The Ni and Al atoms have a spin moment of $0.32\,\mu_B$ and $-0.07\,\mu_B$ in the FM $L2_1$ phase, respectively, resulting in a total moment of $3.89\,\mu_B$ per formula unit. This value is in good agreement with the values reported earlier in the literature, namely, in $4.02\,\mu_B$ [15] and $4.10\,\mu_B$ [16]. Remarkably, however, the Mn moments in Ref. [16] are systematically larger by about $0.2 - 0.3\,\mu_B$ as compared to our values, which is most probably the consequence that in Ref. [16] the generalized gradient approximation was used for the exchange-correlation potential.

TABLE I. Calculated spin magnetic moments (in units of μ_B) of site and antisite Mn atoms, Ni atoms, and site Al atoms in $Ni_2(Mn_{1-x}Al_x)(Al_{1-x}Mn_x)$ alloys for different values of x. The total spin magnetic moments are also shown. Each entry corresponds to the respective magnetic ground state, i.e., to the FM state for $x = 0$ and to the AFM state for $x > 0$.

x	$m^{\rm Mn}_{\rm site}$	$m^{\rm Mn}_{\rm antisite}$	$m^{\rm Ni}$	$m^{\rm Al}_{\rm site}$	$m^{\rm total}$
0.0	3.32	-	0.32	− 0.07	3.89
0.1	3.32	− 3.46	0.26	− 0.06	3.10
0.2	3.32	− 3.43	0.19	− 0.05	2.30
0.3	3.32	− 3.40	0.13	− 0.04	1.49
0.4	3.34	− 3.37	0.06	− 0.03	0.75
0.5	3.35	− 3.35	0	0	0

As can be noticed, the size of the spin moments of the Ni atoms decreases from the $L2_1$ to the $B2$ phase almost proportional with the concentration x. In the $B2$ phase, the two intermixed Mn-Al sublattices become equivalent by symmetry, therefore, the site and antisite Mn moments are equal in magnitude. Concomitantly, the Ni atoms (and also the Al atoms) loose their spin moments and the system becomes a compensated antiferromagnet. From these observations we conclude that in this system the Ni atoms experience induced spin-polarization, and their spin moment strongly depends on the orientational configuration of the strong (stable) Mn moments, thus, also on the temperature.

B. Exchange parameters in the $L2_1$ phase

In the ordered $L2_1$ structure, we calculated the exchange interactions between the Mn atoms both from the FM ground state by using the RTM and from the paramagnetic DLM state by using the SCE technique. The exchange parameters are presented in Fig. 3 as a function of the distance between the Mn atoms. The exchange parameters obtained in the FM state are ferromagnetic up to the fifth shell, while those in the sixth and seventh shells are antiferromagnetic, but relatively small in magnitude. Thus the ferromagnetic character prevails for the Mn-Mn interactions.

In order to check the numerical accuracy of our results, we also performed calculations of the exchange interactions by increasing the angular momentum cutoff to $\ell_{\rm max} = 3$. We found insignificant changes in the dominating nearest-neighbor interactions, while larger deviations occurred only in case of some far (fifth and ninth) neighbors. These changes in the exchange parameters resulted in a decrease by 15 K in the simulated critical temperature (see below). Considering a factor of two in the magnitudes due to the different definitions of the spin model, our calculated interactions are in remarkably good agreement with the couplings determined from a frozen magnon approach [16].

The exchange parameters derived from the DLM state show an overall similarity to those derived from the FM

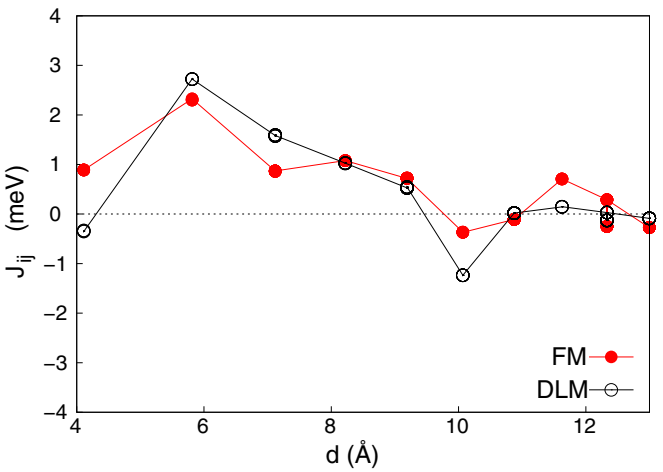

FIG. 3. (Color online) Mn-Mn interactions in Ni_2MnAl in the $L2_1$ phase as a function of the interatomic distance as obtained from the FM and the DLM state.

state. Considerable differences can be seen for the first and the sixth shells, where the couplings in the DLM state show a pronounced AFM tendency. Nevertheless, the magnetic ground state triggered by the interactions from the DLM state is still ferromagnetic.

We performed Monte Carlo simulations with both sets of exchange interactions. By using the parameters derived from the FM and the DLM states, we obtained the transition temperatures $T_C^{FM} = 240$ K and $T_C^{DLM} = 230$ K, respectively. These values are significantly smaller than the experimental one, $T_C^{exp} = 373$ K [8] indicating that the calculated FM Mn-Mn interactions are not sufficiently large in magnitude. Interestingly, the transition temperature, $T_C = 485$ K, derived theoretically in Ref. [14] is twice as large as our values obtained from Monte Carlo simulations, even remarkably larger than the experimental value. Most likely, the random phase approximation (RPA)[37] they used overestimates the Curie temperature. This is corroborated by the fact that Ref. [16] reported $T_C = 368$ K also using RPA, though, as mentioned above, the calculated interactions were very similar to our J_{ij}^{FM} values.

Another quantity closely related to the exchange interactions is the spin-stiffness constant. The spin-stiffness constant D is defined from the low-wave-number limit of the spin-wave energy, $E(\mathbf{q}) = Dq^2$, and, in case of a cubic lattice, it can be expressed as [18,37,38]

$$D = \frac{\mu_B}{3M} \sum_j J_{0j} R_{0j}^2 , \tag{3}$$

where R_{0j} is the distance between sites 0 and j and M the magnitude of the local magnetic moment. Since the above sum is very slowly converging, an exponential decay, $\exp(-\eta R_{0j}/a_{\text{latt}})$, can be introduced and the limit $\eta \to +0$ should be taken [37]. We thus derived the spin stiffness constant by calculating D for different values of η and extrapolated them to $\eta = 0$. For the parameters from the FM and the DLM states, we obtained $D^{FM} = 247$ meV Å^2 and $D^{DLM} = 290$ meV Å^2, respectively. In particular, D^{DLM} compares remarkably well with the one determined from self-consistent spin-spiral calculations, $D = 294$ meV Å^2 [14].

So far, we neglected the influence of the induced moments of the Ni atoms on the magnetic properties of the system at finite temperatures. There have been made quite a few attempts to include the longitudinal fluctuations of the weak moments into the Heisenberg spin model [19,39–41]. Here, we employed a strategy introduced in Ref. [19] to obtain renormalized exchange interactions for the strong (Mn) moments. The method relies on the assumption that the formation of an induced moment at site ν, $\vec{m}_\nu$, is subject to an energy gain,

$$\mathcal{H}_\nu[\{\vec{e}_i\},\vec{m}_\nu] = -\sum_i \kappa_{i\nu} \vec{e}_i \vec{m}_\nu + a_\nu m_\nu^2 , \tag{4}$$

where, as in Eq. (2), $\vec{e}_i$ denote the orientation of the strong moments, while $\kappa_{i\nu}$ and $a_\mu (> 0)$ are parameters that can be obtained from constrained self-consistent electronic structure calculations. Adding the sum of these terms to the Heisenberg model (2) one gets a spin model with the statistical variables, $\vec{e}_i$ and $\vec{m}_\nu$, that can be treated in extended Monte Carlo simulations [19,42,43] to describe the finite temperature equilibrium states of the system. Alternatively, the weak moments' degrees of freedom can be eliminated (integrated out) from the partition function in order to regain a Heisenberg Hamiltonian for the strong moments with renormalized interactions [19],

$$\tilde{J}_{ij} = J_{ij} + \Delta J_{ij} , \quad \Delta J_{ij} = \sum_\nu \frac{\kappa_{i\nu}\kappa_{j\nu}}{2a_\nu} . \tag{5}$$

It should be noted that the expectation values and correlation functions of the strong moments are equivalent within the original model (containing the strong and weak moments' degrees of freedom) and within the renormalized model for the strong moments only [19].

Minimizing the energy (4) with respect to $\vec{m}_\nu$ yields the equilibrium value of the weak moment,

$$\vec{m}_{\nu,0} = \sum_i \frac{\kappa_{i\nu}}{2a_\nu} \vec{e}_i . \tag{6}$$

Note that the above relationship applies also to the expectation values of the moments at finite temperatures. Moreover, the formation energy (4) of the weak moment can be rewritten as

$$\mathcal{H}_\nu[\{\vec{e}_i\},\vec{m}_\nu] = a_\nu(\vec{m}_\nu - \vec{m}_{\nu,0})^2 + \mathcal{H}_\nu[\{\vec{e}_i\}], \tag{7}$$

where the second term on the right-hand side depends just on the configuration of the strong moments. Clearly, the above two equations form the basis to determine the parameters $\kappa_{i\nu}$ and a_ν from first principles. To do so, we used the simplification as in Ref. [19], namely, we supposed that $\kappa_{i\nu}$ differs from zero only for the nearest-neighbor Mn-Ni pairs (κ). Since all the Ni sites are equivalent, in what follows, we also drop the index ν. Taking the ground state value of the Ni moment, $m_{\text{Ni},0} = 0.32\,\mu_B$, in the $L2_1$ phase, see Table I, we obtain

$$\frac{\kappa}{a} = \frac{2m_{\text{Ni},0}}{N_c} = 0.16\,\mu_B , \tag{8}$$

where $N_c = 4$ is the number of the nearest-neighbor Mn sites next to a Ni atom.

The parameter a can be determined based on Eq. (7) by calculating the total energy of the system as a function of μ around the equilibrium value $m_{\text{Ni},0}$ for a fixed spin configuration $\{\vec{e}_i\}$. Such calculations can be performed in terms of constrained density functional theory (CDFT) [44]. Using a longitudinal constraint, we calculated the dependence of the total energy on the Ni moment in the FM and the DLM state as Fig. 4 shows.

In the FM state, the total energy as a function of the magnitude of the Ni moment is parabolic only in the vicinity of the equilibrium value, $0.32\,\mu_B$. In particular, for moments above $0.35\,\mu_B$, the curve becomes asymmetric, indicating the presence of higher order terms in μ_{Ni}. This clearly contravenes the assumption made in Eq. (4). Nevertheless, we fitted the value of $a^{FM} = 487$ meV$/\mu_B^2$ to the parabolic part of the curve. Using the ratio of κ/a in Eq. (8), we obtain $\kappa^{FM} = 78.0$ meV$/\mu_B$. It can be easily seen that, within the approach we used for $\kappa_{i\nu}$, only the nearest-neighbor Mn-Mn interactions will be renormalized by the value, $\Delta J_{NN}^{FM} = \frac{\kappa^2}{a} = \frac{4am_{\text{Ni},0}^2}{N_c^2} = 12.5$ meV, since the two nearest-neighbor Mn atoms have two common nearest-neighbor Ni atoms.

In the DLM state, the equilibrium Ni moment is zero and, as can be inferred from Fig. 4, the parabolic behavior of

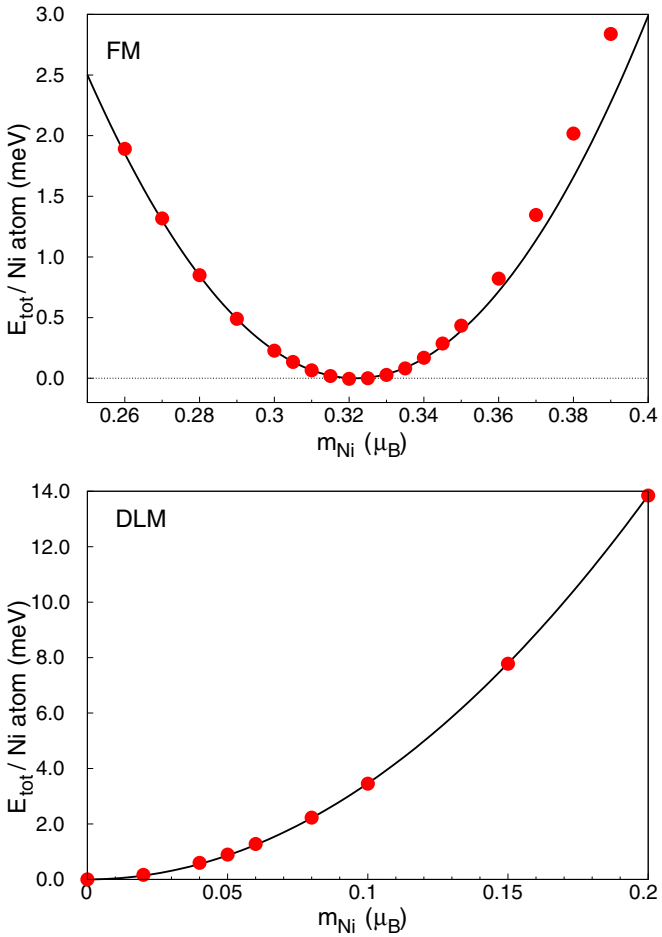

FIG. 4. (Color online) Calculated total energy of Ni_2MnAl in the $L2_1$ phase in the FM (top) and DLM (bottom) state under longitudinal constraint on the Ni moment around the corresponding equilibrium value. The symbols represent the calculated data, the solid line corresponds to a parabolic fit.

the energy applies well for a large range of the constrained moment. The numerical fit resulted in a value of $a^{\mathrm{DLM}} = 346\ \mathrm{meV}/\mu_B^2$, which is clearly smaller than in the FM state. Using again $\kappa/a = 0.16$, we obtain the parameter $\kappa^{\mathrm{DLM}} = 55.4\ \mathrm{meV}/\mu_B$ and a renormalizing term to the NN Mn-Mn interaction, $\Delta J_{\mathrm{NN}}^{\mathrm{DLM}} = 8.87$ meV. We can thus conclude that the formation of local moments at the Ni atoms drastically increases the ferromagnetic coupling between the NN Mn atoms, although this enhancement is remarkably damped in the DLM state. It should be noted that the parameter κ can be related to a Heisenberg-like interaction between the nearest-neighbor Mn and Ni moments, $\kappa = J_{\mathrm{NN}}^{\mathrm{Mn-Ni}}/m_{\mathrm{Mn}}$. Determining the interaction $J_{\mathrm{NN}}^{\mathrm{Mn-Ni}}$ from the FM state using the RTM method, we obtain the value $\kappa = 40.0\ \mathrm{meV}/\mu_B$, which is apparently closer to κ^{DLM} than to κ^{FM}.

In Ref. [19], the renormalized interactions were determined directly from self-consistent spin-spiral calculations and the "bare" interactions were obtained by subtracting the renormalizing corrections, $J_{ij} = \tilde{J}_{ij} - \Delta J_{ij}$. Our present goal is just the opposite, namely, to determine the renormalized interactions through the procedure described in Eqs. (5)–(8). It is thus a subtle question how the bare interactions are defined. Since all the effects of the weak local moments are thought to be covered by the Hamiltonian (4), it is compelling to associate the interactions derived in the DLM state with the bare interactions, since in this state the spin polarization of the Ni atoms is suppressed. To the contrary, due to the large spin-polarization of the Ni atoms in the FM state, the exchange constants derived even from the magnetic force theorem should contain renormalization terms. Moreover, these parameters are also influenced by higher order spin interactions [45], which is not the case for the DLM state, since the multispin interactions provided by the SCE method are, in general, irreducible [29,30].

Choosing the SCE-DLM interactions as the bare couplings, we obtained $\tilde{J}_{\mathrm{NN}} = 12.13$ meV with the renormalization term from FM state, ΔJ^{FM}, and $\tilde{J}_{\mathrm{NN}} = 8.52$ meV with ΔJ^{DLM}. Using the spin model with renormalized NN coupling in the MC simulations, the Curie temperature remarkably increased to $T_{\mathrm{C}} = 730$ K or to $T_{\mathrm{C}} = 600$ K with ΔJ^{DLM}. The inclusion of the longitudinal fluctuations of the Ni moments via the renormalization process proposed in Ref. [19] thus largely overestimates the Curie temperature of Ni_2MnAl in the $L2_1$ phase as compared to the experiment (373 K). Our value for the T_{C} obtained with the renormalized spin-model from the DLM state is, however, comparable to that reported in Ref. [14] (485 K).

C. Exchange interactions for the disordered alloys

In order to study the change in the magnetic structure from the ordered $L2_1$ phase to the disordered $B2$ state, we calculated the exchange interactions between the Mn atoms in the (partially) disordered alloys $Ni_2(Mn_{1-x}Al_x)$ $(Al_{1-x}Mn_x)$ as a function of x. Here, we employed the RTM method for the AFM ground state of the alloys ($x > 0$), in which the site and antisite Mn atoms exhibit opposite spin orientation. In Fig. 5, the calculated isotropic Mn-Mn interactions are shown as sorted out according to the sublattice (site and antisite) positions of the Mn atoms. Although we calculated the exchange parameters up to the 15th shell, as what follows, we shall present and discuss only the first three NN interactions.

Considering only the site positions of the Mn atoms, see upper panel of Fig. 5, the ferromagnetic NN coupling is decreasing with increasing disorder and above $x = 0.2$ it becomes antiferromagnetic, reaching a value of about -1.2 meV in the $B2$ phase ($x = 0.5$). A similar tendency can be observed for the large ferromagnetic second NN interaction, however, this coupling remains ferromagnetic (0.8 meV) in the $B2$ phase. The third NN coupling slightly increases with increasing disorder, and above $x = 0.2$ it saturates at about 1.4 meV. It can then be concluded that the overall ferromagnetic coupling of the site Mn moments is preserved with the disorder.

Disorder between the Mn and Al species introduces new types of Mn-Mn interactions that can influence the magnetic ground state. One set of them are the couplings between the Mn atoms occupying the pristine Al sites (antisite Mn atoms). For small disorder, the rather large antiferromagnetic NN interaction dominates and it shows fairly small changes against disorder. The ferromagnetic second and third NN interactions increase with increasing x from small values ($0.2 - 0.3$ meV), but the second NN interaction slightly decreases again for $x > 0.25$. As clear from the middle panel of Fig. 5, in the

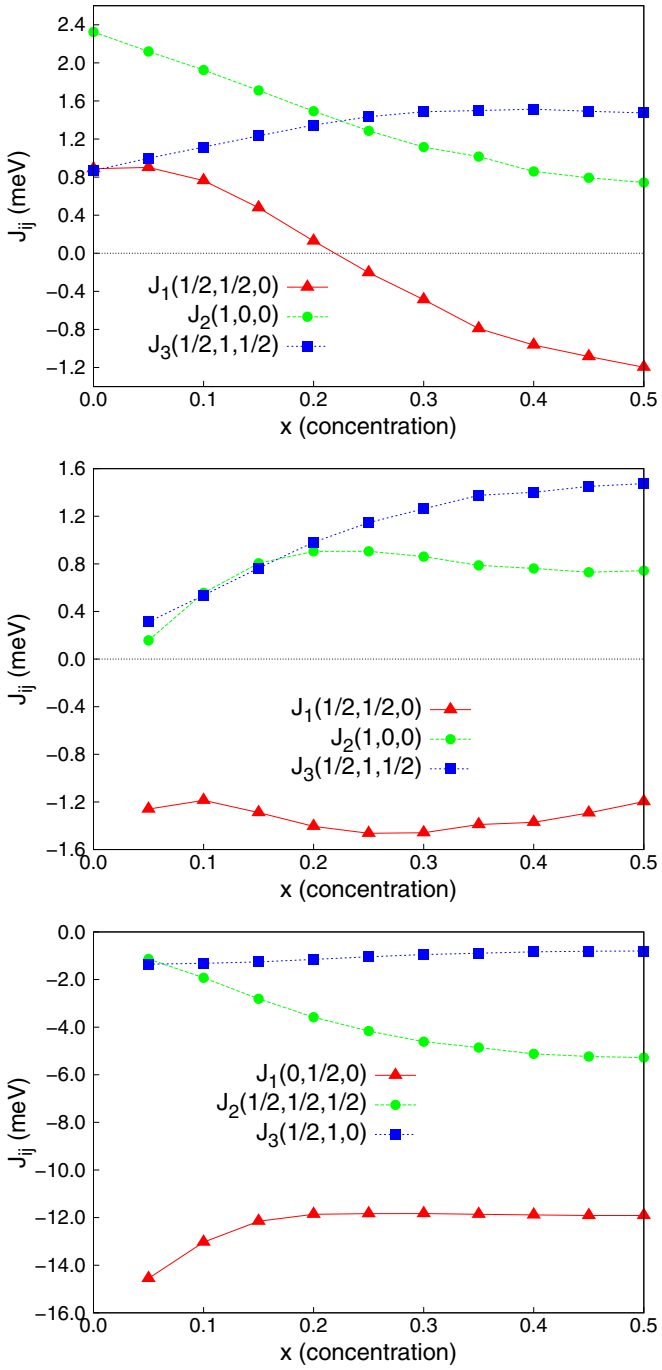

FIG. 5. (Color online) Calculated first (J_1), second (J_2), and third (J_3) nearest-neighbor Mn-Mn interactions as a function of the degree of disorder x in $Ni_2(Mn_{1-x}AL_x)(Al_{1-x}Mn_x)$ alloys. Top: site-site pairs, middle: antisite-antisite pairs, and bottom: site-antisite pairs. The representative crystallographic position of the pairs is also given with the label of the interactions, see Fig. 1.

$B2$ phase the corresponding site–site and antisite-antisite interactions take the same values since the two sublattices become equivalent.

The calculated isotropic exchange interactions between two Mn atoms, one of them located in the pristine Mn (site) and the other one in the pristine Al sublattice (antisite), are plotted in the lower panel of Fig. 5. Apparently, all presented (first, second and third nearest-neighbor) couplings are antiferromagnetic in the whole range of x, and, in particular, the first and second NN interactions are significantly larger in magnitude than the exchange couplings discussed before, being ~ -12 and ~ -5 meV in the $B2$ phase, respectively. These interactions show monotonous changes with x, but above $x > 0.2-0.3$, they are practically unaffected by the increase of disorder.

As regard the large antiferromagnetic first NN site Mn-antisite Mn coupling, there is a good quantitative agreement between our results and those obtained for the artificial $B2$-I and $B2$-II structures in Ref. [16]. Our calculations confirm that the change in the magnetic structure from FM to AFM is primarily due to the appearance of (1/2,0,0) Mn-Mn pairs, i.e., with a distance of $a/2$, in samples with any disorder. Indeed, the energy difference between the AFM and FM states of the $B2$ phase calculated just by taking into account these interactions in the spin model (2) yields -35.7 meV/unit cell, which compares remarkably well with the energy difference obtained from the total energy calculations, -36.65 meV/unit cell. It should also be mentioned that the AFM order is somewhat weakened by the antiferromagnetic (1/2,1/2,0) interactions, but it is strengthened via the antiferromagnetic (1/2,1/2,1/2) interactions, see also Fig. 1.

Using the calculated isotropic exchange interactions, we performed Monte Carlo simulations to study the finite temperature magnetic properties in the $B2$ phase. In particular, we evaluated the spin-spin correlation functions that provide important information about the magnetic short range order in the system. For the nth nearest-neighbor shell, the spin-spin correlation function is defined as

$$c(n) = \frac{1}{N}\sum_i \frac{1}{N_n}\sum_{\vec{R}_n} \langle \vec{e}_{\vec{R}_i}\, \vec{e}_{\vec{R}_i+\vec{R}_n} \rangle, \qquad (9)$$

where $\langle \dots \rangle$ denotes the statistical average, $\vec{R}_i$ are translation vectors of the lattice, among them $\vec{R}_n$ span the nth shell. N stands for the number of translation vectors considered in the calculations and N_n is the number of sites forming the nth shell.

The temperature dependence of the calculated spin-spin correlation functions in the disordered $B2$ phase is displayed in Fig. 6. The first-shell site-site (and also antisite-antisite) spin-spin correlation function approaches to $+1$ at low temperatures, which reflects ferromagnetic ordering within each of the two disordered sublattices. Quite clearly, this applies to $c(n)$ for any n with respect to a given sublattice. For finite temperatures, the site-site $c(1)$ remains positive signaling FM order, but for higher temperatures it approaches zero. The temperature of the magnetic order–disorder transition is identified with the position of the inflection point of $c(n)$. The spin-spin correlation functions related to site-antisite pairs are negative, at low temperature approaching -1, which implies that the site and antisite Mn moments have opposite directions in the ground state. These correlation functions also tend to zero, but, as can be seen in Fig. 6, after the inflection point, the decay of $c(1)$ and $c(2)$ is much slower than that of the other correlation functions, and they seem to preserve a finite value far beyond the order-disorder transition temperature. This is the signal for a strong short-range magnetic ordering (AFM correlation) in the paramagnetic phase due to the large

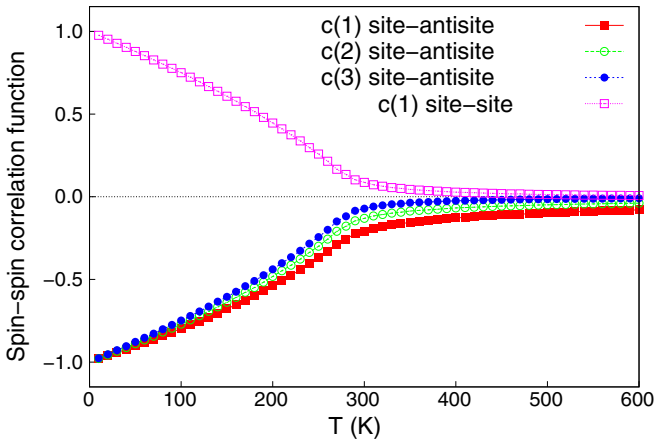

FIG. 6. (Color online) Temperature dependence of selected spin-spin correlation functions, Eq. (9), of Ni_2MnAl in the disordered $B2$ phase. Presented are the site-site correlation functions for the first shell, and the site-antisite correlation functions for the first three shell.

antiferromagnetic site-antisite exchange interactions. Note that for the $B2$ phase, we obtained a transition temperature of $T_C^{B2} = 270$ K, which agrees well with the experimental value of 313 K [8].

D. Magnetic anisotropy energies

Based on the magnetic force theorem, we determined the magnetic anisotropy energy (MAE) in the $B2$ phase under tetragonal distortion along [001] (c axis). Note that we also changed the lattice constant a in order to keep the volume of the unit cell constant. Table II shows the calculated magnetic anisotropy energies for some values of the c/a ratio. Bear in mind that a negative sign of the MAE corresponds to an easy plane normal to [001], while positive MAE's refer to an easy axis parallel to [001].

Due to the cubic symmetry, the MAE as defined in Eq. (1) is zero for $c/a = 1$. Clearly from Table II, the easy direction can be tuned by tetragonal distortion: in case of compression ($c/a < 0$), the easy axis is along the c axis, while for stretching ($c/a > 0$), the preferred direction is in the plane normal to the c axis. It also can be inferred that the magnitude of MAE changes almost proportionally with the c/a ratio. Note that small tetragonal compression in the equilibrium geometric structure, $c/a = 0.991$, was reported theoretically [15]. According to our results, this implies an easy c axis with a magnitude of about 0.05 meV/unit cell $\simeq 16 \times 10^5 \mathrm{J/m^3}$ for the MAE. Note that this value is only about one-third of the uniaxial anisotropy constant of hcp Co and by two orders less in magnitude than the effective anisotropy constant found theoretically in the frustrated antiferromagnet $IrMn_3$ [46].

TABLE II. Calculated magnetic anisotropy energies per unit cell E_{anis}, based on the magnetic force theorem (1), for some values of the c/a ratio in the $B2$ phase of Ni_2MnAl.

c/a	E_{anis} (meV)
0.90	0.054
0.95	0.027
1.00	0.000
1.05	−0.028
1.10	−0.059

Finally, we notice that, due to tetragonal symmetry, the AFM pseudophases, $B2$-I and $B2$-II, exhibit uniaxial MAE even without distorting the lattice ($c = a$). Considering the AFM ground states reported in Ref. [16], for the $B2$-I structure, we determined an easy-plane anisotropy with a MAE of -0.19 meV (-62.0×10^5 J/m^3), while the preferred magnetic orientation for the $B2$-II structure was found along the c axis with a MAE of 0.14 meV (45.7×10^5 J/m^3). This observation implies that a short-range chemical ordering, which might occur in the disordered $B2$ phase, can significantly influence the MAE of the system.

IV. CONCLUSIONS

We performed detailed first-principles analysis for the full-Heusler Ni_2MnAl alloy focusing on the interrelation between the long-range chemical disorder with respect to the Mn and Al atoms and the magnetic structure. From the self-consistent calculations, we found that the ground state of the system is the ferromagnetic $L2_1$ phase and any disorder among the Mn and Al atoms causes an antiferromagnetic order for the site and antisite Mn atoms. The site and antisite Mn moments are highly stable against disorder and in the fully disordered $B2$ phase their magnitudes become equal, implying a compensated AFM ordering in this phase. The Ni atoms exhibit weak induced moments as they decrease nearly proportionally with increasing disorder and disappear in the $B2$ phase.

In the $L2_1$ phase, we calculated the isotropic exchange parameters between the Mn atoms from the ferromagnetic ground state and from the paramagnetic DLM state, in good agreement with previous theoretical results [16]. From Monte Carlo simulations, we, however, obtained a Curie temperature significantly smaller than the experimentally one. We made an attempt to include the longitudinal fluctuations of the Ni moments into the spin model by employing the renormalization technique proposed in Ref. [19]. As expected, we obtained a remarkable increase of the ferromagnetic nearest-neighbor Mn-Mn coupling mediated by the induced Ni moments, but this procedure largely overestimated the Curie temperature. This might indicate that in this system the Mn and Ni moments can not be treated as individual degrees of freedom.

We also investigated the exchange interactions between the Mn atoms with increasing long-range disorder. In accordance with Ref. [16], we found that the transition of the magnetic structure from FM in the $L2_1$ phase to AFM in the $B2$ phase is primarily triggered by the appearance of Mn-Mn pairs with a distance of $a/2$, that display a strong antiferromagnetic coupling. Based on the Mn-Mn interactions, for the $B2$ phase we determined a Néel temperature in good agreement with experiment. From the calculated spin-spin correlation functions we established a bipartite AFM ground state in the $B2$ phase. Above the transition temperature, we found finite spin-spin correlations for the first and second shell of site-antisite Mn pairs, indicating strong short-range antiferromagnetic correlations in the paramagnetic phase.

Finally, we calculated the magnetic anisotropy energy for the tetragonally distorted $B2$ phase and established a

spin-reorientation transition with respect to the compressed and stretched samples. At 9% compression found in first-principles calculations [15], the magnitude of the calculated anisotropy energy amounted about 0.05 meV per unit cell, while the $B2$-I or $B2$-II types of chemical orderings increased the magnitude of the MAE by a factor of about three. Nevertheless, it remains quite ambiguous whether this MAE is sufficient to stabilize the AFM state in potential exchange bias devices.

ACKNOWLEDGMENTS

The research leading to the presented results received funding from the European Union Seventh Framework Programme (FP7/2007-2013) under Grant Agreement No. NMP3-SL-2013-604398. Financial support was also provided by the Hungarian Scientific Research Fund under Contract OTKA K115575.

[1] B. G. Park, J. Wunderlich, X. Martí, V. Holý, Y. Kurosaki, M. Yamada, H. Yamamoto, A. Nishide, J. Hayakawa, H. Takahashi *et al.*, Nat. Mater. **10**, 347 (2011).
[2] A. B. Shick, S. Khmelevskyi, O. N. Mryasov, J. Wunderlich, and T. Jungwirth, Phys. Rev. B **81**, 212409 (2010).
[3] N. Fukatani, K. Inagaki, T. Miyawaki, K. Ueda, and H. Asano, J. Appl. Phys. **113**, 17C103 (2013).
[4] N. Fukatani, H. Fujita, T. Miyawaki, K. Ueda, and H. Asano, J. Korean Phys. Soc. **63**, 711 (2013).
[5] K.-U. Neumann, T. Ohoyama, N. Yamada, and K. Ziebeck, *Alloys and Compounds of d-Elements with Main Group Elements. Part 2* (Springer-Verlag, Berlin, 2001).
[6] T. Kanomata, M. Kikuchi, and H. Yamauchi, J. Alloys Compd. **414**, 1 (2006).
[7] S. Khmelevskyi, E. Simon, and L. Szunyogh, Phys. Rev. B **91**, 094432 (2015).
[8] M. Acet, E. Duman, E. F. Wassermann, L. Maosa, and A. Planes, J. Appl. Phys. **92**, 3867 (2002).
[9] T. Mehaddene, J. Neuhaus, W. Petry, K. Hradil, P. Bourges, and A. Hiess, Phys. Rev. B **78**, 104110 (2008).
[10] F. Gejima, Y. Sutou, R. Kainuma, and K. Ishida, Metall. Mater. Trans. A **30**, 2721 (1999).
[11] S. Morito, T. Kakeshita, K. Hirata, and K. Otsuka, Acta Mater. **46**, 5377 (1998).
[12] R. Kainuma, K. Ishida, and H. Nakano, Metall. Mater. Trans. A **27**, 4153 (1996).
[13] A. Vovk, M. Yu, L. Malkinski, C. OConnor, Z. Wang, E. Durant, J. Tang, and V. Golub, J. Appl. Phys. **99**, 08R503, (2006).
[14] J. Enkovaara, A. Ayuela, J. Jalkanen, L. Nordström, and R. M. Nieminen, Phys. Rev. B **67**, 054417 (2003).
[15] T. Büsgen, J. Feydt, R. Hassdorf, S. Thienhaus, M. Moske, M. Boese, A. Zayak, and P. Entel, Phys. Rev. B **70**, 014111 (2004).
[16] I. Galanakis and E. Şaşıoğlu, App. Phys. Lett. **98**, 102514 (2011).
[17] M. Asato, M. Ohkubo, T. Hoshino, F. Nakamura, N. Fujima, and H. Tatsuoka, Mater. Trans. **49**, 1760 (2008).
[18] A. Liechtenstein, M. Katsnelson, V. Antropov, and V. Gubanov, J. Magn. Magn. Mater. **67**, 65 (1987).
[19] M. Ležaić, P. Mavropoulos, G. Bihlmayer, and S. Blügel, Phys. Rev. B **88**, 134403 (2013).
[20] L. Szunyogh, B. Újfalussy, P. Weinberger, and J. Kollár, Phys. Rev. B **49**, 2721 (1994).
[21] R. Zeller, P. H. Dederichs, B. Újfalussy, L. Szunyogh, and P. Weinberger, Phys. Rev. B **52**, 8807 (1995).
[22] S. H. Vosko, L. Wilk, and M. Nusair, Can. J. Phys. **58**, 1200 (1980).
[23] G. H. O. Daalderop, P. J. Kelly, and M. F. H. Schuurmans, Phys. Rev. B **41**, 11919 (1990).
[24] L. Szunyogh, B. Újfalussy, and P. Weinberger, Phys. Rev. B **51**, 9552 (1995).
[25] H. J. F. Jansen, Phys. Rev. B **59**, 4699 (1999).
[26] B. Lazarovits, L. Szunyogh, P. Weinberger, and B. Újfalussy, Phys. Rev. B **68**, 024433 (2003).
[27] L. Udvardi, L. Szunyogh, K. Palotás, and P. Weinberger, Phys. Rev. B **68**, 104436 (2003).
[28] H. Ebert and S. Mankovsky, Phys. Rev. B **79**, 045209 (2009).
[29] R. Drautz and M. Fähnle, Phys. Rev. B **69**, 104404 (2004).
[30] R. Drautz and M. Fähnle, Phys. Rev. B **72**, 212405 (2005).
[31] B. L. Gyorffy, A. J. Pindor, J. Staunton, G. M. Stocks, and H. Winter, J. Phys. F: Met. Phys. **15**, 1337 (1985).
[32] J. B. Staunton, L. Szunyogh, A. Buruzs, B. L. Gyorffy, S. Ostanin, and L. Udvardi, Phys. Rev. B **74**, 144411 (2006).
[33] J. B. Staunton, S. Ostanin, S. S. A. Razee, B. L. Gyorffy, L. Szunyogh, B. Ginatempo, and E. Bruno, Phys. Rev. Lett. **93**, 257204 (2004).
[34] L. Szunyogh, L. Udvardi, J. Jackson, U. Nowak, and R. Chantrell, Phys. Rev. B **83**, 024401 (2011).
[35] A. Deák, L. Szunyogh, and B. Újfalussy, Phys. Rev. B **84**, 224413 (2011).
[36] A. Deák, E. Simon, L. Balogh, L. Szunyogh, M. dos Santos Dias, and J. B. Staunton, Phys. Rev. B **89**, 224401 (2014).
[37] M. Pajda, J. Kudrnovsky, I. Turek, V. Drchal, and P. Bruno, Phys. Rev. B **64**, 174402 (2001).
[38] J. Thoene, S. Stanislav Chadov, G. Fecher, C. Felser, and J. Kübler, J. Phys. D: Appl. Phys. **42**, 084013 (2009).
[39] O. N. Mryasov, Phase Trans. **78**, 197 (2005).
[40] S. Polesya, S. Mankovsky, O. Sipr, W. Meindl, C. Strunk, and H. Ebert, Phys. Rev. B **82**, 214409 (2010).
[41] L. M. Sandratskii, R. Singer, and E. Şaşıoğlu, Phys. Rev. B **76**, 184406 (2007).
[42] N. M. Rosengaard and B. Johansson, Phys. Rev. B **55**, 14975 (1997).
[43] A. V. Ruban, S. Khmelevskyi, P. Mohn, and B. Johansson, Phys. Rev. B **75**, 054402 (2007).
[44] P. H. Dederichs, S. Blügel, R. Zeller, and H. Akai, Phys. Rev. Lett. **53**, 2512 (1984).
[45] S. Lounis and P. H. Dederichs, Phys. Rev. B **82**, 180404 (2010).
[46] L. Szunyogh, B. Lazarovits, L. Udvardi, J. Jackson, and U. Nowak, Phys. Rev. B **79**, 020403(R) (2009).